

ESTVocoder: An Excitation-Spectral-Transformed Neural Vocoder Conditioned on Mel Spectrogram *

Xiao-Hang Jiang, Hui-Peng Du, Yang Ai[†], Ye-Xin Lu, and Zhen-Hua Ling

National Engineering Research Center of Speech and Language Information
Processing,

University of Science and Technology of China, Hefei, P. R. China
{jiang_xiaohang, redmist}@mail.ustc.edu.cn, yangai@ustc.edu.cn,
yxl0102@mail.ustc.edu.cn, zhling@ustc.edu.cn

Abstract. This paper proposes ESTVocoder, a novel excitation-spectral-transformed neural vocoder within the framework of source-filter theory. The ESTVocoder transforms the amplitude and phase spectra of the excitation into the corresponding speech amplitude and phase spectra using a neural filter whose backbone is ConvNeXt v2 blocks. Finally, the speech waveform is reconstructed through the inverse short-time Fourier transform (ISTFT). The excitation is constructed based on the F0: for voiced segments, it contains full harmonic information, while for unvoiced segments, it is represented by noise. The excitation provides the filter with prior knowledge of the amplitude and phase patterns, expecting to reduce the modeling difficulty compared to conventional neural vocoders. To ensure the fidelity of the synthesized speech, an adversarial training strategy is applied to ESTVocoder with multi-scale and multi-resolution discriminators. Analysis-synthesis and text-to-speech experiments both confirm that our proposed ESTVocoder outperforms or is comparable to other baseline neural vocoders, e.g., HiFi-GAN, SiFi-GAN, and Vocos, in terms of synthesized speech quality, with a reasonable model complexity and generation speed. Additional analysis experiments also demonstrate that the introduced excitation effectively accelerates the model’s convergence process, thanks to the speech spectral prior information contained in the excitation.

Keywords: Neural vocoder · Excitation · Filter · Spectral transformation.

*This work was funded by the National Nature Science Foundation of China under Grant 62301521, the Anhui Provincial Natural Science Foundation under Grant 2308085QF200, and the Fundamental Research Funds for the Central Universities under Grant WK2100000033.

[†]Corresponding author.

1 Introduction

Text-to-speech (TTS) is a technique that utilizes machines to convert written text content into audible speech. With the recent advancements in deep learning, there has been a significant improvement in the clarity and naturalness of synthesized speech. A TTS system typically consists of two key components, i.e., an acoustic model and a vocoder. The acoustic model is responsible for predicting acoustic features (e.g., mel spectrogram) from the input text. Subsequently, the vocoder uses these features to generate the final speech waveform. Besides TTS, other fields such as voice conversion (VC) and singing voice synthesis (SVS) also require a vocoder to reconstruct waveform. Thus, a robust vocoder is crucial for the field of speech signal processing, which is also the focus of this paper.

Traditional vocoders, such as STRAIGHT [28] and WORLD [42], synthesize speech waveform using traditional signal processing methods. Although they are computationally simple and fast, result in synthesized speech with lower naturalness. With the development of deep learning, the WaveNet [46] represents a significant milestone in synthesized speech quality. WaveNet is an autoregressive neural vocoder capable of producing natural and clear speech waveforms. Unlike traditional vocoders that rely on traditional signal processing methods, WaveNet relies entirely on end-to-end neural network training. However, autoregressive neural vocoders generate audio samples sequentially and use previously generated samples to create new ones, leading to extremely low efficiency and high computational complexity. To address the issue of low efficiency in autoregressive models, researchers have proposed various alternative approaches, including knowledge distillation-based models [45,50], flow-based models [52,51], and glottis-based models [26,62]. Although these models have improved inference efficiency, their overall computational complexity remains high.

To overcome the aforementioned issues, non-autoregressive neural vocoders have gradually been proposed. Non-autoregressive models generate all samples in parallel, offering high computational efficiency. For instance, HiFi-GAN [29] vocoder maintains high naturalness in synthesized audio thanks to the generative adversarial network (GAN) [16] based training while balancing high generation speed. However, there is still room for efficiency improvement with these vocoders, as they directly predict high-temporal-resolution waveforms from input acoustic features. The substantial discrepancy in time resolution between the acoustic features and waveforms, results in extensive upsampling operations on the acoustic features, leading to significant computational demands. Thus, subsequent neural vocoders have adopted the approach of predicting amplitude and phase spectrum and then reconstructing the waveform using the inverse short-time Fourier transform (ISTFT). For instance, Vocos [59] with ConvNeXt blocks [35] as backbone, directly predicts the amplitude and phase spectrum at the same temporal resolution from the input acoustic features, thereby maintaining the same feature resolution at all frame rates. Vocos has increased its generation speed by more than tenfold compared to HiFi-GAN while maintaining high-quality synthesized speech.

Most of the aforementioned vocoders only use the mel spectrogram as input, which is convenient, but the mel spectrogram is a compressed representation of the amplitude spectrum and may lose some acoustic details. Therefore, many vocoders that utilize other acoustic features have also been proposed. A common approach is to enhance vocoder performance based on the source-filter theory framework by introducing the F0 as an additional acoustic feature. Neural source filter (NSF) model [65] is a pioneer in applying neural networks within the source-filter framework, which synthesizes speech waveform directly based on explicit F0 and mel spectrograms. Recently, some works combining source-filter vocoders with GAN-based training, such as SiFi-GAN [71] and SF-GAN [37], have been proposed. This type of vocoders generates excitation based on the F0. The excitation waveform is then processed through a neural filter conditioned on the mel spectrogram to directly produce the final speech waveform. Experiments have shown that after introducing the additional F0 features, the quality of the speech generated by these vocoders is obviously improved. However, their excitations are often constructed based on single F0, lacking harmonic information, which may impact the reconstruction performance of the neural filter. In addition, these methods often rely on direct transformation of the excitation waveform, still leaving room for improvements in efficiency and model complexity. Excitation-spectral-transformed methods in source-filter-based neural vocoders have not yet been thoroughly investigated.

To achieve high-fidelity speech synthesis as well as efficient training and rapid generation speed, we propose a novel excitation-spectral-transformed neural vocoder called ESTVocoder. The ESTVocoder is designed based on the source-filter theory and first produces an excitation according to the F0. Compared to the single-F0-based excitation used by SiFi-GAN [71] and SF-GAN [37], the proposed ESTVocoder utilizes a full-harmonic excitation which contains richer spectral information. Subsequently, a neural filter with ConvNeXt v2 blocks [67] as the backbone transforms the amplitude and phase spectra of the excitation into the corresponding amplitude and phase spectra of the speech, conditioned on the mel spectrogram. Finally, the speech waveform is reconstructed via ISTFT. Both analysis-synthesis and TTS experimental results show that our proposed ESTVocoder outperforms or is comparable to HiFi-GAN, SiFi-GAN, and Vocos, in terms of synthesized speech quality. Our proposed ESTVocoder also has an extremely fast training convergence speed, thanks to the introduction of spectral prior information contained in the excitation.

This paper is organized as follows: In Section 2, we provide details on our proposed ESTVocoder. In Section 3, we present our experimental results. Finally, we give conclusions in Section 4.

2 Proposed Method

2.1 Overview

Fig. 1 shows an overview of the proposed ESTVocoder model. In ESTVocoder, the F0 sequence $\mathbf{f} \in \mathbb{R}^F$ first passes through an excitation producer to produce

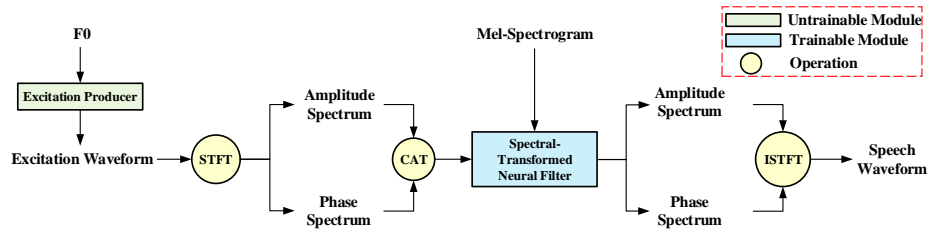


Fig. 1: Overview of the proposed ESTVocoder. Here, CAT represents the concatenation operation.

an excitation waveform $e \in \mathbb{R}^T$, i.e.,

$$e = EP(\mathbf{f}, S_r), \quad (1)$$

where EP represents the excitation producer and S_r is waveform sampling rate. F and T denote the number of frames of the F_0 and the number of excitation waveform samples, respectively. Assuming the frame shift for extracting F_0 and spectral features from the waveform is w_s , it holds $T = F \cdot w_s$. Then, a spectral-transformed neural filter transforms the amplitude spectrum $\mathbf{A}_e \in \mathbb{R}^{F \times N}$ and phase spectrum $\mathbf{P}_e \in \mathbb{R}^{F \times N}$ extracted from the excitation waveform e by STFT into the corresponding speech amplitude spectrum $\hat{\mathbf{A}} \in \mathbb{R}^{F \times N}$ and phase spectrum $\hat{\mathbf{P}} \in \mathbb{R}^{F \times N}$, with the mel spectrogram $\mathbf{M} \in \mathbb{R}^{F \times M}$ as conditions, i.e.,

$$\mathbf{A}_e, \mathbf{P}_e = STFT(e), \quad (2)$$

$$\hat{\mathbf{A}}, \hat{\mathbf{P}} = ST-NF(\mathbf{A}_e, \mathbf{P}_e | \mathbf{M}), \quad (3)$$

where $ST-NF$ denotes the spectral-transformed neural filter. N and M represent the number of the frequency bins of the amplitude/phase spectra and mel spectrogram, respectively. Finally, the predicted speech amplitude and phase spectra are reconstructed into the speech waveform $\hat{x} \in \mathbb{R}^T$ through the ISTFT, i.e.,

$$\hat{x} = ISTFT(\hat{\mathbf{A}} \cdot \exp(j\hat{\mathbf{P}})). \quad (4)$$

2.2 Excitation Producer

The excitation producer generates the corresponding excitation waveform e based on the frame-level F_0 sequence \mathbf{f} . First, a point-level F_0 sequence $\mathbf{f}_{pl} = [f_1, \dots, f_T]^T$ is first generated by repeating the F_0 value of \mathbf{f} within each frame, which then serves as the input to the excitation producer. The excitation producer outputs an excitation signal $e = [e_1, \dots, e_T]^T$, which is a sine-based signal at voiced segments and Gaussian white noise at unvoiced segments. Specifically, the excitation waveform can be represented as:

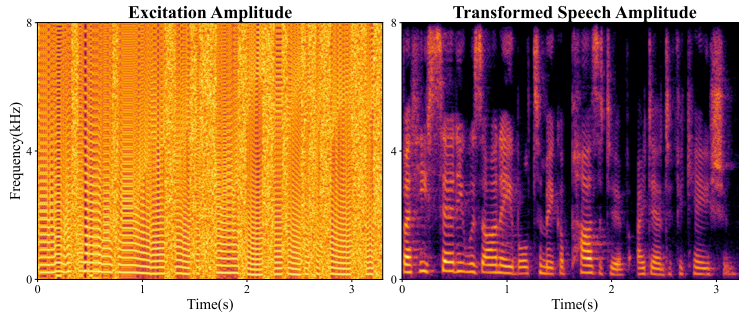


Fig. 2: Visualization of the amplitude spectrum of the excitation waveform and the speech waveform generated by ESTVocoder.

$$e_t = \begin{cases} \sum_{k=1}^K \alpha \sin\left(\sum_{h=1}^t 2\pi k \frac{f_h}{S_r}\right) + n_t, & f_t > 0, t \in V_j \\ \frac{1}{3\sigma} n_t, & f_t = 0 \end{cases}, \quad (5)$$

where $K = \lfloor \frac{S_r/2}{\min(f)} \rfloor$ represents the minimum number of harmonics required to cover the entire frequency band. $f_t = 0$ indicates that the t -th sampling point is part of an unvoiced frame, $n_t \sim \mathcal{N}(0, \sigma^2)$ is a Gaussian noise, V_j represents the j -th voiced segment to which the t -th sampling point belongs, α and σ are hyperparameters.

The left subplot of Fig. 2 gives a visualization example of the amplitude spectrum of the excitation waveform. Compared to previous works [37,2], the most significant difference in our proposed excitation is that our excitation includes all possible harmonic information. In this way, the produced excitation already includes the basic acoustic pattern of the speech waveform, expecting to effectively alleviate the modeling and learning difficulty for the subsequent neural filter.

2.3 Spectral-Transformed Neural Filter

Unlike the waveform-transformed neural filters used in other vocoders, the neural filter in ESTVocoder transforms the amplitude spectrum \mathbf{A}_e and phase spectrum \mathbf{P}_e of the excitation waveform e into the speech amplitude spectrum $\hat{\mathbf{A}}$ and phase spectrum $\hat{\mathbf{P}}$ conditioned on the mel spectrogram \mathbf{M} , and then reconstructs the speech waveform \hat{x} through ISTFT. Fig. 2 provides an visualization example of amplitude spectral transformation (from the left subplot to the right subplot). Therefore, the role of the neural filter is to achieve the gradual spectral refinement using a neural network, guided by the information from the mel spectrogram. As mentioned in Section 2.2, the excitation spectrum already has the rudiments of the speech spectrum, essentially providing the neural filter with prior spectral information. We expect that such an excitation can reduce the

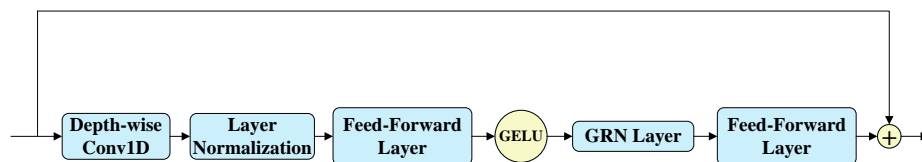


Fig. 3: The specific compositional structure of the ConvNeXt v2 block.

learning difficulty of the neural filter model, thereby accelerating the model’s convergence speed, while also diminishing the smooth artificial artifacts in the amplitude and phase spectra of the synthesized speech.

Specifically, the amplitude and phase spectra of the excitation are concatenated along the dimensional axis and then passed through a dimension-reduction layer. The mel-spectrogram, used as a condition, is first injected into a dimension-expansion layer to match the dimension of the dimension-reduced amplitude-phase feature. Then, these two features with same dimension are added together and passed through the backbone network (i.e., ConvNeXt v2) along with a layer normalization layer and a feed-forward layer to predict the speech amplitude and phase spectra. Inspired by Vocos [59], we split the output of the above feed-forward layer into two features along the dimensional axis. One feature generates the amplitude spectrum through exponential activation, while the other feature generates the phase spectrum by first applying sine/cosine calculations and then the atan2 function.

The neural filter adopts a ConvNeXt v2 [67] as its backbone, which has been proven to possess superior modeling capabilities compared to the commonly used ResNet networks [20] in HiFi-GAN [29] and the ConvNeXt network [35] in Vocos [59]. The backbone ConvNeXt v2 network consists of multiple cascaded identical ConvNeXt v2 blocks. As shown in Fig. 3, the key components of the ConvNeXt v2 block include a 1D depth convolutional layer, a layer normalization layer, a feed-forward layer that projects features to higher dimensions, a Gaussian Error Linear Unit (GELU) activation [21], a global response normalization (GRN) layer [67], and an another feed-forward layer that projects features back to their original dimensions. The GRN layer comprises three integral steps, i.e., aggregating global features, normalizing these features, and calibrating them, thereby enhancing feature diversity and ultimately boosting the representational quality. The final output of the ConvNeXt v2 block is obtained by adding the input of the 1D depth convolutional layer and the output of the last feed-forward layer (i.e., residual connection).

2.4 Training Criteria

In ESTVocoder, only the neural network filter contains trainable parameters, and it is trained using an adversarial training approach. The ESTVocoder uses multi-period discriminator (MPD) [29] and multi-resolution discriminator (MRD) [25] for adversarial training to ensure the quality of synthesized waveforms.

- **MPD**: The MPD consists of 5 parallel sub-MPDs that operate in parallel. Each sub-MPD converts the input synthesized waveform $\hat{\mathbf{x}}$ or natural waveform \mathbf{x} into a 2D periodic map based on the preset period. This mapping result then goes through a series of 5 consecutive processing stages, each stage containing a layer of 2D convolution and a leaky rectified linear unit (LReLU) activation function. The final output of the processing chain is further processed through a 2D convolutional output layer to generate discriminative scores. The period parameters are set to 2, 3, 5, 7, and 11, respectively.
- **MRD**: The MRD is configured with 3 parallel sub-MRDs. Each sub-MRD uses the amplitude spectrum extracted from $\hat{\mathbf{x}}$ or \mathbf{x} as input, based on specific STFT parameters. Assuming the STFT parameters for extracting the input amplitude and phase spectrum for the neural filter are: [frame length, frame shift, FFT point number] = [w_l , w_s , $2N + 1$]. We set the STFT parameters for the three sub-MRDs as [$w_l/2$, $w_s/2$, $(2N + 1)/2$], [w_l , w_s , $2N + 1$] and [$2w_l$, $2w_s$, $2(2N + 1)$], respectively. Each sub-MRD consists of blocks made up of 2D convolutional layer and LReLU activation, followed by a 2D convolutional layer that provides the final output.

We use the hinge form of adversarial loss. Assuming D^* represents the sub-discriminator of MPD or MRD, the corresponding generator adversarial loss and discriminator adversarial loss are as follows.

$$\mathcal{L}_{adv-G}^* = \mathbb{E}_{\hat{\mathbf{x}}} \max(0, 1 - D^*(\hat{\mathbf{x}})), \quad (6)$$

$$\mathcal{L}_{adv-D}^* = \mathbb{E}_{(\hat{\mathbf{x}}, \mathbf{x})} [\max(0, 1 - D^*(\mathbf{x})) + \max(0, 1 + D^*(\hat{\mathbf{x}}))]. \quad (7)$$

Additionally, feature matching loss \mathcal{L}_{FM}^* [31] is also utilized, characterized by the summation of the mean absolute error (MAE) between the corresponding intermediate layer outputs of sub-discriminator D^* when provided with inputs $\hat{\mathbf{x}}$ or \mathbf{x} .

In addition, we also incorporate the mean absolute error (MAE) loss on the mel spectrogram between the extracted mel spectrogram $\hat{\mathbf{M}}$ and natural one \mathbf{M} derived from synthesized waveform $\hat{\mathbf{x}}$ and natural one \mathbf{x} , respectively, i.e.,

$$\mathcal{L}_M = \frac{1}{FM} \cdot \mathbb{E}_{(\hat{\mathbf{M}}, \mathbf{M})} \left(\left\| \hat{\mathbf{M}} - \mathbf{M} \right\|_1 \right). \quad (8)$$

Therefore, the final GAN-based losses for generator (i.e., the neural filter) and discriminator (i.e., the MPD and MRD) are respectively defined by the following expressions.

$$\mathcal{L}_G = \sum_{i=1}^5 (\mathcal{L}_{adv-G}^{Pi} + \mathcal{L}_{FM}^{Pi}) + \lambda_{MRD} \sum_{j=1}^3 (\mathcal{L}_{adv-G}^{Rj} + \mathcal{L}_{FM}^{Rj}) + \lambda_M \mathcal{L}_M, \quad (9)$$

$$\mathcal{L}_D = \sum_{i=1}^5 \mathcal{L}_{adv-D}^{Pi} + \lambda_{MRD} \sum_{j=1}^3 \mathcal{L}_{adv-D}^{Rj}, \quad (10)$$

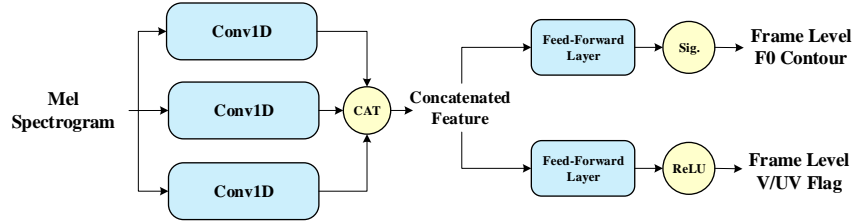


Fig. 4: The structure of the F0 predictor. Here, *CAT* and *Sig.* represents the concatenation operation and sigmoid activation.

where P_i and R_j represent i -th sub-MPD and j -th sub-MRD, λ_{MRD} and λ_M are hyperparameters. The training process follows the standard training mode of GAN, i.e., using \mathcal{L}_G and \mathcal{L}_D to train the generator and discriminator alternately.

2.5 Analysis-synthesis and TTS applications

During the test stage, we apply the proposed ESTVocoder on two tasks, i.e., the analysis-synthesis task and TTS task. The process of analysis-synthesis applications is consistent with the training process. We first extract the natural F0 and the natural mel spectrogram from the natural speech and then inject them into the well-trained ESTVocoder to generate the speech waveform.

In TTS tasks, after predicting the mel spectrogram from text via an acoustic model, we use an F0 predictor [37] to predict the F0 from the mel spectrograms. Then the predicted F0 and mel spectrogram are inject into the well-trained ESTVocoder to generate the speech waveform. The structure of the F0 predictor is shown in Fig. 4. The mel spectrogram is first input into three parallel convolutional layers with different kernel sizes to obtain three sets of intermediate features. Subsequently, the concatenated features are inputted into two parallel feed-forward layers with different activation functions (Sigmoid and ReLU, respectively) to separately derive the F0 contour and the voiced/unvoiced (V/UV) flag. Finally, multiply the F0 contour and the V/UV flag to obtain the final F0 sequence.

3 Experiments

3.1 Experimental Setup

Dataset and Implementation. We conducted experiments on the LJSpeech [24] dataset, which included 13,100 speech utterances from an English female for a total of approximately 24 hours. All speech waveforms were downsampled to 16 kHz for our experiments. We randomly selected 10,480 utterances for training, 1,310 for validation, and remaining 1,310 for testing. When performing the

STFT, the frame length was 640 (i.e., $w_l = 640$), the frame shift was 160 (i.e., $w_s = 160$), and the number of FFT points was 1024 (i.e., $N = 513$).

In the neural filter model, before the ConvNeXt v2 block, both the layer dimension-reduction and dimension-expansion layers had 512 nodes. The number of ConvNeXt v2 blocks in the ConvNeXt v2 network was set to 8. For each ConvNeXt v2 block, the kernel size and channel size were set to 7 and 512, respectively. The model was trained on a single NVIDIA RTX TITAN GPU and optimized using the AdamW optimizer with $\beta_1 = 0.8$, $\beta_2 = 0.99$, and weight decay of 0.01. The learning rate was set initially to 2×10^{-4} and scheduled to decay with a factor of 0.999 at every epoch.

Baselines. We compared ESTVocoder with HiFi-GAN [29]¹, SiFi-GAN [71]² and Vocos [59]³. SiFi-GAN introduces excitation into HiFi-GAN, constructing a neural vocoder within the source-filter framework. In contrast to HiFi-GAN and SiFi-GAN, Vocos models the amplitude and phase spectra instead of directly modeling the waveform. However, it is not designed within the source-filter framework. Therefore, comparing them with the proposed ESTVocoder is fair and reasonable. All the baseline models were trained on the same LJSpeech dataset with the same training environment as ESTVocoder.

Tasks. In this paper, we conducted analysis-synthesis experiments on HiFi-GAN, SiFi-GAN, Vocos, and ESTVocoder. We performed TTS experiments only on HiFi-GAN, Vocos, and ESTVocoder using mel spectrograms predicted by FastSpeech2 [54]⁴. Since SiFi-GAN utilized mel cepstral features extracted by WORLD [42] and no TTS experiments were conducted in the original paper [71], we also discarded the TTS experiment on SiFi-GAN.

Evaluation metrics. For the analysis-synthesis experiment, we have adopted a variety of objective metrics to evaluate the quality of synthesized speech from multiple perspectives. To evaluate the amplitude-related quality, the root mean square error of logarithmic amplitude spectrum (LAS-RMSE) and mel cepstrum distortion (MCD) were used. To evaluate the F0 modeling accuracy, root mean square error of F0 (F0-RMSE) and V/UV flag error (denoted by V/UV) were adopted. Finally, to comprehensively evaluate the quality of synthesized speech, we introduced two commonly used tools, including perceptual evaluation of speech quality (PESQ) [53] and virtual speech quality objective listener (ViSQOL) [10].

To evaluate the generation efficiency of vocoders, we compared the real-time factor (RTF) and training speed. The RTF is calculated as the ratio of generation time and the actual duration of the test set. The training speed is defined as the seconds taken to complete one epoch of training (s/e), which reflects the efficiency of model training.

¹<https://github.com/jik876/hifi-gan>.

²<https://github.com/chomeyama/SiFi-GAN>.

³<https://github.com/gemelo-ai/vocos>.

⁴<https://github.com/ming024/FastSpeech2>.

Table 1: Quality-related objective evaluation results of for ESTVocoder, HiFi-GAN, SiFi-GAN and Vocos on the test set of the LJSpeech for the analysis-synthesis experiments. The **bold** and underline numbers indicate the optimal and sub-optimal results, respectively.

	LAS-RMSE (dB)↓	MCD (dB)↓	F0-RMSE (cent)↓	V/UV (%)↓	PESQ↑	ViSQOL↑
ESTVocoder	<u>36.51</u>	0.931	4.17	4.99	3.70	4.895
HiFi-GAN	40.34	1.227	5.07	5.23	3.48	4.815
SiFi-GAN	29.39	1.252	5.03	<u>5.15</u>	3.33	4.703
Vocos	39.07	<u>1.033</u>	<u>4.40</u>	5.31	<u>3.51</u>	<u>4.863</u>

Table 2: Efficiency-related objective evaluation results of for ESTVocoder, HiFi-GAN, SiFi-GAN and Vocos on the test set of the LJSpeech for the analysis-synthesis experiments. The **bold** and underline numbers indicate the optimal and sub-optimal results, respectively. Here, s/e represents second per epoch and " $a\times$ " represents $a\times$ real time.

	RTF (GPU)↓	RTF (CPU)↓	Training Speed (s/e)↓
ESTVocoder	0.0016 (625.0×)	0.0112 (89.3×)	<u>203</u>
HiFi-GAN	<u>0.0013</u> (769.2×)	0.1496 (6.8×)	358
SiFi-GAN	0.0135 (74.1×)	0.1568 (6.4×)	567
Vocos	0.0009 (1111.1×)	0.0093 (107.5×)	199

For the TTS experiment, we employed a subjective mean opinion score (MOS) test, to compare the naturalness of the vocoders. In each MOS test, 20 test utterances synthesized by compared vocoders along with the natural utterances were compared and evaluated by at least 30 native English listeners. This test was conducted on the Amazon Mechanical Turk crowd-sourcing platform, where listeners were asked to rate the naturalness on a scale from 1 to 5, with a score interval of 0.5.

3.2 Evaluation Results⁵

The quality-related objective evaluation results of the proposed ESTVocoder and baseline HiFi-GAN, SiFi-GAN and Vocos for the analysis-synthesis experiments are presented in Table 1. Regarding the amplitude quality, it can be observed that our proposed ESTVocoder achieved the lowest MCD results, but it was second only to SiFi-GAN in the LAS-RMSE metric. However, the MCD calculation is performed in the mel domain, which better reflects human perception. Therefore, it can be inferred that the synthesized speech of

⁵Audio samples of the proposed ESTVocoder can be accessed at <https://pb20000090.github.io/NCMMSC2024/>.

Table 3: Subjective evaluation results of ESTVocoder, HiFi-GAN and Vocos on the test set of the LJSpeech for the TTS experiments.

	MOS \uparrow
Natural	4.01 \pm 0.044
ESTVocoder	3.87 \pm 0.051
HiFi-GAN	3.90 \pm 0.047
Vocos	3.87 \pm 0.049

our proposed ESTVocoder had higher perceived quality. For F0 recovery capability, our proposed ESTVocoder had the lowest F0-RMSE and V/UV error, indicating its strong F0 restoration capability and fewer pronunciation errors. Thanks to ESTVocoder’s excellent performance in amplitude spectrum perceptual quality and fundamental frequency recovery capability, it is unsurprising that its overall speech quality is also the best, according to PESQ and ViSQOL results. Therefore, our proposed ESTVocoder outperformed commonly used waveform-prediction-based neural vocoders (i.e., HiFi-GAN), excitation-waveform-transformed neural vocoders (e.g., SiFi-GAN), and spectral-prediction-based neural vocoders (i.e., Vocos) in terms of synthesized speech quality. This confirms the advantages of our proposed excitation spectral transformation method.

Table 2 gives the results of the comparison of the generation and training speeds among the proposed ESTVocoder, HiFi-GAN, SiFi-GAN and Vocos for the analysis-synthesis experiments. We first compared the proposed ESTVocoder with Vocos, as both were designed to predict spectra rather than waveforms. The generation and training efficiency of ESTVocoder were slightly lower than those of Vocos, which is reasonable given that ESTVocoder introduced an additional excitation producer module. This conclusion is consistent with the comparison between HiFi-GAN and SiFi-GAN. When compared with the two waveform-prediction-based neural vocoders, i.e., HiFi-GAN and SiFi-GAN, although our proposed ESTVocoder had a slightly slower generation speed on GPU compared to HiFi-GAN, its generation speed on CPU was significantly faster than both HiFi-GAN and SiFi-GAN. This demonstrates the efficiency advantage of predicting spectra rather than waveforms, especially when GPU parallel acceleration is not available. Additionally, the training efficiency of ESTVocoder is also significantly higher than that of HiFi-GAN and SiFi-GAN.

For TTS experiments, the results of the subjective MOS test on the natural speech and speeches generated by ESTVocoder, HiFi-GAN and Vocos are shown in Table 3. We can see that their average MOS was similar. To determine the significance of the differences among them, we also calculated the p -value of the t -test. The results of the two t -tests between ESTVocoder and HiFi-GAN and between ESTVocoder and Vocos indicated that the performance differences between the ESTVocoder and other baseline vocoders were not significant ($p > 0.05$) in the TTS task. Therefore, our proposed ESTVocoder is comparable to other baseline vocoders in terms of subjective quality on TTS tasks. However, it

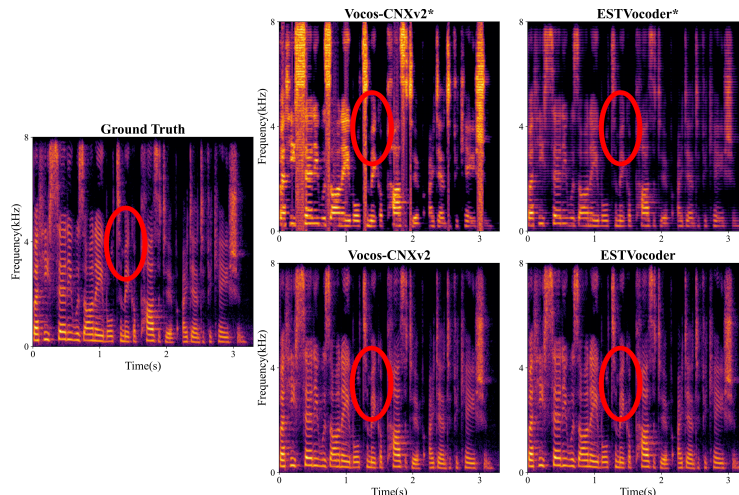


Fig. 5: Visualized amplitude spectra of natural speech and speeches generated by Vocos-CNXv2*, ESTVocoder*, Vocos-CNXv2 and ESTVocoder (example sentence LJ034-0143)

Table 4: Quality-related objective evaluation results of for ESTVocoder, ESTVocoder-CNXv1, Vocos-CNXv2 and Vocos on the test set of the LJSpeech for the analysis-synthesis experiments.

	LAS-RMSE	MCD	F0-RMSE	V/UV	PESQ \uparrow	ViSQOL \uparrow
	(Hz) \downarrow	(dB) \downarrow	(dB) \downarrow	(%) \downarrow		
ESTVocoder	36.51	0.931	4.17	4.99	3.70	4.895
ESTVocoder-CNXv1	37.60	1.025	4.27	5.46	3.63	4.880
Vocos-CNXv2	38.53	0.998	4.30	5.30	3.58	4.878
Vocos	39.07	1.033	4.40	5.31	3.51	4.863

achieves better objective results in analysis-synthesis tasks and has considerable training and generation speed advantages. In the following subsection, we also demonstrate that ESTVocoder has a faster training convergence speed, thus saving training costs, which is also one of its advantages.

3.3 Analysis and Discussion

Discussion on backbone. Choosing a good backbone is crucial for the performance of the synthesized speech by a neural vocoder. As mentioned in Section 2.3, we choose ConvNeXt v2 blocks as the backbone for our proposed ESTVocoder due to their proven strong modeling capabilities. However, Vocos uses ConvNeXt blocks as its backbone.

Although researchers have systematically compared the differences between ConvNeXt and ConvNeXt v2 in the field of image processing [67], this difference

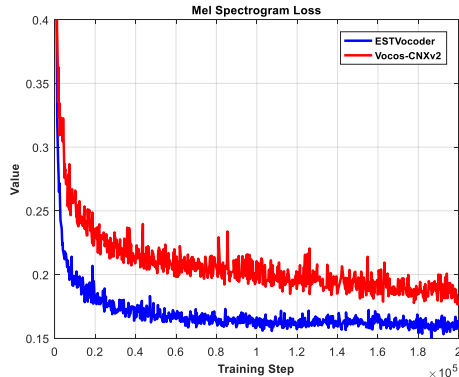


Fig. 6: Training curves of mel-spectrogram loss for ESTVocoder and Vocos-CNXv2.

has yet to be systematically validated in the field of speech signal processing. Therefore, we replaced all ConvNeXt v2 blocks in ESTVocoder with ConvNeXt blocks (referred to as ESTVocoder-CNXv1) and compared it with the original ESTVocoder. Simultaneously, we replaced all ConvNeXt blocks in Vocos with ConvNeXt v2 blocks (referred to as Vocos-CNXv2) and compared it with the original Vocos. Objective experimental results are listed in Table 4. We can observe that in all metrics, the ESTVocoder outperformed the ESTVocoder-CNXv1, and the Vocos-CNXv2 outperformed the Vocos. This result indicates that ConvNeXt v2 has a stronger modeling capability in vocoder tasks compared to ConvNeXt, which is why we chose ConvNeXt v2 as the backbone for ESTVocoder.

Analysis of the role of the excitation producer. As mentioned in Section 2.2, the original intention of introducing the excitation spectra in ESTVocoder is to provide the neural filter with prior information about the speech spectra, thereby reducing the training difficulty of the neural filter and improving the quality of the synthesized speech. To confirm this point, we compared ESTVocoder with Vocos-CNXv2. They both use ConvNeXt v2 as the backbone, so Vocos-CNXv2 can be approximately regarded as the ablated version of ESTVocoder without the excitation producer. We conducted the following three analyses. 1) Objective evaluation. As shown in Table 4, the ESTVocoder outperformed the Vocos-CNXv2 for all objective metrics. This confirms that the introduced excitation producer significantly helps improve the quality of synthesized speech. 2) Visual analysis. Both ESTVocoder and Vocos-CNXv2 used 8 ConvNeXt v2 blocks, so we attempted to reconstruct the speech waveform based on the output from their 4th block (referred to as ESTVocoder* and Vocos-CNXv2*, respectively) to test their performance at intermediate stages of the model. Figure 5 shows the amplitude spectra of the speeches generated by Vocos-CNXv2*, ESTVocoder*, Vocos-CNXv2, and ESTVocoder. Interestingly,

the amplitude spectrum of ESTVocoder* is close to that of natural speech, while the amplitude spectrum of Vocos-CNXv2* is significantly worse. This indicates that the speech spectral prior introduced by the excitation allows the neural filter to quickly learn the shape of the speech spectra, resulting in a faster learning speed. By comparing Vocos-CNXv2 and ESTVocoder, as shown by the red circles in Figure 5, ESTVocoder’s harmonic restoration is more accurate, which is also attributed to the introduction of the excitation prior information. 3) Convergence speed analysis. Figure 6 plots the training curves of the mel spectrogram loss for Vocos-CNXv2 and ESTVocoder. From the figure, we can also see that ESTVocoder’s convergence speed is significantly faster, which is also attributed to the excitation prior information provided to the neural filter.

4 Conclusions

In this paper, we present an excitation-spectral-transformed neural vocoder called ESTVocoder under the source-filter framework. An excitation producer produces the excitation waveform according to F0, and then the neural filter transforms the excitation amplitude and phase spectra to speech ones conditioned on the mel spectrogram. The comprehensive experimental results demonstrate that our proposed ESTVocoder outperforms several baseline vocoders. Analysis experiments confirm that the excitation provides the neural filter with speech spectral priors, effectively reducing the training difficulty of the neural filter and improving the quality of synthesized speech. Further improving the efficiency of ESTVocoder and applying it to other tasks (i.e., speech enhancement) will be the focus of our future work.

References

1. Yang Ai, Xiao-Hang Jiang, Ye-Xin Lu, Hui-Peng Du, and Zhen-Hua Ling. Apcodec: A neural audio codec with parallel amplitude and phase spectrum encoding and decoding. *arXiv preprint arXiv:2402.10533*, 2024.
2. Yang Ai and Zhen-Hua Ling. A neural vocoder with hierarchical generation of amplitude and phase spectra for statistical parametric speech synthesis. *IEEE/ACM Transactions on Audio, Speech, and Language Processing*, 28:839–851, 2020.
3. Yang Ai and Zhen-Hua Ling. APNet: An all-frame-level neural vocoder incorporating direct prediction of amplitude and phase spectra. *IEEE/ACM Transactions on Audio, Speech, and Language Processing*, 2023.
4. Yang Ai and Zhen-Hua Ling. Neural speech phase prediction based on parallel estimation architecture and anti-wrapping losses. In *Proc. ICASSP*, pages 1–5, 2023.
5. Yang Ai, Ye-Xin Lu, and Zhen-Hua Ling. Long-frame-shift neural speech phase prediction with spectral continuity enhancement and interpolation error compensation. *IEEE Signal Processing Letters*, 2023.
6. Alexei Baevski, Steffen Schneider, and Michael Auli. vq-wav2vec: Self-supervised learning of discrete speech representations. *arXiv preprint arXiv:1910.05453*, 2019.
7. Zalán Borsos, Raphaël Marinier, Damien Vincent, Eugene Kharonov, Olivier Pietquin, Matt Sharifi, Dominik Roblek, Olivier Teboul, David Grangier, Marco

- Tagliasacchi, et al. Audiolm: a language modeling approach to audio generation. *IEEE/ACM Transactions on Audio, Speech, and Language Processing*, 2023.
8. Karlheinz Brandenburg and Gerhard Stoll. Iso/mpeg-1 audio: A generic standard for coding of high-quality digital audio. *Journal of the Audio Engineering Society*, 42(10):780–792, 1994.
 9. Sabine Buchholz and Javier Latorre. Crowdsourcing preference tests, and how to detect cheating. In *Twelfth Annual Conference of the International Speech Communication Association*, 2011.
 10. Michael Chinen, Felicia SC Lim, Jan Skoglund, Nikita Gureev, Feargus O’Gorman, and Andrew Hines. ViSQOL v3: An open source production ready objective speech and audio metric. In *Proc. QoMEX*, pages 1–6, 2020.
 11. Alexandre Défossez, Jade Copet, Gabriel Synnaeve, and Yossi Adi. High fidelity neural audio compression. *Transactions on Machine Learning Research*, 2023.
 12. Martin Dietz, Markus Multrus, Vaclav Eksler, Vladimir Malenovsky, Erik Norvell, Harald Pobloth, Lei Miao, Zhe Wang, Lasse Laaksonen, Adriana Vasilache, et al. Overview of the evs codec architecture. In *2015 IEEE International Conference on Acoustics, Speech and Signal Processing (ICASSP)*, pages 5698–5702. IEEE, 2015.
 13. Chris Donahue, Julian McAuley, and Miller Puckette. Adversarial audio synthesis. In *Proc. ICLR*, 2018.
 14. Chenpeng Du, Yiwei Guo, Xie Chen, and Kai Yu. Vqtts: High-fidelity text-to-speech synthesis with self-supervised vq acoustic feature. *arXiv preprint arXiv:2204.00768*, 2022.
 15. Hui-Peng Du, Ye-Xin Lu, Yang Ai, and Zhen-Hua Ling. Apnet2: High-quality and high-efficiency neural vocoder with direct prediction of amplitude and phase spectra. In *National Conference on Man-Machine Speech Communication*, pages 66–80. Springer, 2023.
 16. Ian Goodfellow, Jean Pouget-Abadie, Mehdi Mirza, Bing Xu, David Warde-Farley, Sherjil Ozair, Aaron Courville, and Yoshua Bengio. Generative adversarial nets. In *Proc. NeurIPS*, volume 27, 2014.
 17. Alex Graves and Alex Graves. Long short-term memory. *Supervised sequence labelling with recurrent neural networks*, pages 37–45, 2012.
 18. Alexey Gritsenko, Tim Salimans, Rianne van den Berg, Jasper Snoek, and Nal Kalchbrenner. A spectral energy distance for parallel speech synthesis. In *Proc. NeurIPS*, volume 33, pages 13062–13072, 2020.
 19. Haohan Guo, Fenglong Xie, Frank K Soong, Xixin Wu, and Helen Meng. A multi-stage multi-codebook vq-vae approach to high-performance neural tts. *arXiv preprint arXiv:2209.10887*, 2022.
 20. Kaiming He, Xiangyu Zhang, Shaoqing Ren, and Jian Sun. Deep residual learning for image recognition. In *Proceedings of the IEEE conference on computer vision and pattern recognition*, pages 770–778, 2016.
 21. Dan Hendrycks and Kevin Gimpel. Gaussian error linear units (GELUs). In *Proc. ICML*, volume 70, pages 3441–3450, 2017.
 22. Wei-Ning Hsu, Benjamin Bolte, Yao-Hung Hubert Tsai, Kushal Lakhotia, Ruslan Salakhutdinov, and Abdelrahman Mohamed. Hubert: Self-supervised speech representation learning by masked prediction of hidden units. *IEEE/ACM Transactions on Audio, Speech, and Language Processing*, 29:3451–3460, 2021.
 23. Zhichao Huang, Chutong Meng, and Tom Ko. Repcodec: A speech representation codec for speech tokenization. *arXiv preprint arXiv:2309.00169*, 2023.
 24. Keith Ito and Linda Johnson. The LJ speech dataset. <https://keithito.com/LJ-Speech-Dataset>, 2017.

25. Wonsung Jang, Dongwook Lim, Jiyoung Yoon, and et al. Univnet: A neural vocoder with multi-resolution spectrogram discriminators for high-fidelity waveform generation. In *Proc. Interspeech*, 2021.
26. Lauri Juvola, Bajibabu Bollepalli, Vassilis Tsiaras, and Paavo Alku. GlotNet—a raw waveform model for the glottal excitation in statistical parametric speech synthesis. *IEEE/ACM Transactions on Audio, Speech, and Language Processing*, 27(6):1019–1030, 2019.
27. Takuhiro Kaneko, Kou Tanaka, Hirokazu Kameoka, and Shogo Seki. iSTFTNet: Fast and lightweight mel-spectrogram vocoder incorporating inverse short-time Fourier transform. In *Proc. ICASSP*, pages 6207–6211, 2022.
28. Hideki Kawahara, Ikuyo Masuda-Katsuse, and Alain De Cheveigne. Restructuring speech representations using a pitch-adaptive time-frequency smoothing and an instantaneous-frequency-based f0 extraction: Possible role of a repetitive structure in sounds. *Speech communication*, 27(3-4):187–207, 1999.
29. Jungil Kong, Jaehyeon Kim, and Jaekyoung Bae. HiFi-GAN: Generative adversarial networks for efficient and high fidelity speech synthesis. *Proc. NeurIPS*, 33:17022–17033, 2020.
30. Peter Kroon, E Deprettere, and R Sluyter. Regular-pulse excitation—a novel approach to effective and efficient multipulse coding of speech. *IEEE transactions on acoustics, speech, and signal processing*, 34(5):1054–1063, 1986.
31. Kundan Kumar, Rithesh Kumar, Thibault de Boissiere, Lucas Gestin, Wei Zhen Teoh, Jose Sotelo, Alexandre de Brebisson, Yoshua Bengio, and Aaron Courville. MelGAN: generative adversarial networks for conditional waveform synthesis. In *Proc. NeurIPS*, pages 14910–14921, 2019.
32. Junhyeok Lee, Seungu Han, Hyunjae Cho, and Wonbin Jung. PHASEAUG: A differentiable augmentation for speech synthesis to simulate one-to-many mapping. In *Proc. ICASSP*, pages 1–5, 2023.
33. Haohe Liu, Woosung Choi, Xubo Liu, Qiuqiang Kong, Qiao Tian, and DeLiang Wang. Neural vocoder is all you need for speech super-resolution, 2022.
34. Songxiang Liu, Dan Su, and Dong Yu. Diffgan-tts: High-fidelity and efficient text-to-speech with denoising diffusion gans. *arXiv preprint arXiv:2201.11972*, 2022.
35. Zhuang Liu, Hanzi Mao, Chao-Yuan Wu, Christoph Feichtenhofer, Trevor Darrell, and Saining Xie. A convnet for the 2020s. In *Proc. CVPR*, pages 11976–11986, 2022.
36. Ilya Loshchilov and Frank Hutter. Decoupled weight decay regularization. In *Proc. ICLR*, 2018.
37. Ye-Xin Lu, Yang Ai, and Zhen-Hua Ling. Source-filter-based generative adversarial neural vocoder for high fidelity speech synthesis. In *National Conference on Man-Machine Speech Communication*, pages 68–80. Springer, 2022.
38. Ye-Xin Lu, Yang Ai, and Zhen-Hua Ling. Mp-senet: A speech enhancement model with parallel denoising of magnitude and phase spectra. *arXiv preprint arXiv:2305.13686*, 2023.
39. Andrew L Maas, Awni Y Hannun, and Andrew Y Ng. Rectifier nonlinearities improve neural network acoustic models. In *Proc. ICML*, volume 30, page 3, 2013.
40. Soroush Mehri, Kundan Kumar, Ishaan Gulrajani, Rithesh Kumar, Shubham Jain, Jose Sotelo, Aaron Courville, and Yoshua Bengio. SampleRNN: An unconditional end-to-end neural audio generation model. In *Proc. ICLR*, 2016.
41. Fabian Mentzer, David Minnen, Eirikur Agustsson, and Michael Tschannen. Finite scalar quantization: Vq-vae made simple. In *The Twelfth International Conference on Learning Representations*, 2023.

42. Masanori Morise, Fumiya Yokomori, and Kenji Ozawa. WORLD: A vocoder-based high-quality speech synthesis system for real-time applications. *IEICE Transactions on Information and Systems*, 99(7):1877–1884, 2016.
43. Paarth Neekhara, Chris Donahue, Miller Puckette, Shlomo Dubnov, and Julian McAuley. Expediting tts synthesis with adversarial vocoding. In *Proc. Interspeech*, volume 2019, pages 186–190, 2019.
44. Tu Anh Nguyen, Wei-Ning Hsu, Antony d’Avirro, Bowen Shi, Itai Gat, Maryam Fazel-Zarani, Tal Remez, Jade Copet, Gabriel Synnaeve, Michael Hassid, et al. Expresso: A benchmark and analysis of discrete expressive speech resynthesis. *arXiv preprint arXiv:2308.05725*, 2023.
45. Aaron Oord, Yazhe Li, Igor Babuschkin, Karen Simonyan, Oriol Vinyals, Koray Kavukcuoglu, George Driessche, Edward Lockhart, Luis Cobo, Florian Stimberg, et al. Parallel WaveNet: Fast high-fidelity speech synthesis. In *Proc. ICML*, pages 3918–3926, 2018.
46. Aaron van den Oord, Sander Dieleman, Heiga Zen, Karen Simonyan, Oriol Vinyals, Alex Graves, Nal Kalchbrenner, Andrew Senior, and Koray Kavukcuoglu. WaveNet: A generative model for raw audio. In *Proc. SSW*, pages 125–125, 2016.
47. Douglas O’Shaughnessy. Linear predictive coding. *IEEE potentials*, 7(1):29–32, 1988.
48. Keisuke Oyamada, Hirokazu Kameoka, Takuhiro Kaneko, Kou Tanaka, Nobukatsu Hojo, and Hiroyasu Ando. Generative adversarial network-based approach to signal reconstruction from magnitude spectrogram. In *Proc. EUSIPCO*, pages 2514–2518, 2018.
49. Blanca Pena and Luofeng Huang. Wave-gan: a deep learning approach for the prediction of nonlinear regular wave loads and run-up on a fixed cylinder. *Coastal Engineering*, 167:103902, 2021.
50. Wei Ping, Kainan Peng, and Jitong Chen. ClariNet: Parallel wave generation in end-to-end text-to-speech. In *Proc. ICLR*, 2018.
51. Wei Ping, Kainan Peng, Kexin Zhao, and Zhao Song. Waveflow: A compact flow-based model for raw audio. In *Proc. ICML*, pages 7706–7716, 2020.
52. Ryan Prenger, Rafael Valle, and Bryan Catanzaro. Waveglow: A flow-based generative network for speech synthesis. In *Proc. ICASSP*, pages 3617–3621, 2019.
53. ITUT Recommendation. P. 862.2: Wideband extension to recommendation P. 862 for the assessment of wideband telephone networks and speech codecs. *International Telecommunication Union*, 2007.
54. Yi Ren, Chenxu Hu, Xu Tan, Tao Qin, Sheng Zhao, Zhou Zhao, and Tie-Yan Liu. FastSpeech 2: Fast and high-quality end-to-end text to speech. In *Proc. ICLR*, 2020.
55. Yong Ren, Tao Wang, Jiangyan Yi, Le Xu, Jianhua Tao, Chu Yuan Zhang, and Junzuo Zhou. Fewer-token neural speech codec with time-invariant codes. In *ICASSP 2024-2024 IEEE International Conference on Acoustics, Speech and Signal Processing (ICASSP)*, pages 12737–12741. IEEE, 2024.
56. Takaaki Saeki, Detai Xin, Wataru Nakata, Tomoki Koriyama, Shinnosuke Takamichi, and Hiroshi Saruwatari. Utmos: Utokyo-sarulab system for voicemos challenge 2022. *Interspeech 2022*, 2022.
57. Redwan Salami, Claude Laflamme, J-P Adoul, and Dominique Massaloux. A toll quality 8 kb/s speech codec for the personal communications system (pcs). *IEEE Transactions on Vehicular Technology*, 43(3):808–816, 1994.
58. Jonathan Shen, Ruoming Pang, Ron J Weiss, Mike Schuster, Navdeep Jaitly, Zongheng Yang, Zhifeng Chen, Yu Zhang, Yuxuan Wang, Rj Skerrv-Ryan, et al.

- Natural TTS synthesis by conditioning WaveNet on mel spectrogram predictions. In *Proc. ICASSP*, pages 4779–4783, 2018.
59. Hubert Siuzdak. Vocos: Closing the gap between time-domain and fourier-based neural vocoders for high-quality audio synthesis. *arXiv preprint arXiv:2306.00814*, 2023.
 60. Thomas Tremain. Linear predictive coding systems. In *ICASSP’76. IEEE International Conference on Acoustics, Speech, and Signal Processing*, volume 1, pages 474–478. IEEE, 1976.
 61. Jean-Marc Valin, Gregory Maxwell, Timothy B Terriberry, and Koen Vos. High-quality, low-delay music coding in the opus codec. In *Audio Engineering Society Convention 135*. Audio Engineering Society, 2013.
 62. Jean-Marc Valin and Jan Skoglund. LPCNet: Improving neural speech synthesis through linear prediction. In *Proc. ICASSP*, pages 5891–5895, 2019.
 63. A Vasuki and PT Vanathi. A review of vector quantization techniques. *IEEE Potentials*, 25(4):39–47, 2006.
 64. Chengyi Wang, Sanyuan Chen, Yu Wu, Ziqiang Zhang, Long Zhou, Shujie Liu, Zhuo Chen, Yanqing Liu, Huaming Wang, Jinyu Li, et al. Neural codec language models are zero-shot text to speech synthesizers.(2023). *arXiv preprint arXiv:2301.02111*, 2023.
 65. Xin Wang, Shinji Takaki, and Junichi Yamagishi. Neural source-filter-based waveform model for statistical parametric speech synthesis. In *Proc. ICASSP*, pages 5916–5920, 2019.
 66. Yuxuan Wang, RJ Skerry-Ryan, Daisy Stanton, Yonghui Wu, Ron J Weiss, Navdeep Jaitly, Zongheng Yang, Ying Xiao, Zhifeng Chen, Samy Bengio, et al. Tacotron: Towards end-to-end speech synthesis. *Interspeech 2017*, 2017.
 67. Sanghyun Woo, Shoubhik Debnath, Ronghang Hu, Xinlei Chen, Zhuang Liu, In So Kweon, and Saining Xie. Convnext v2: Co-designing and scaling convnets with masked autoencoders. In *Proc. CVPR*, pages 16133–16142, 2023.
 68. Yi-Chiao Wu, Israel D Gebru, Dejan Marković, and Alexander Richard. Audiodec: An open-source streaming high-fidelity neural audio codec. In *ICASSP 2023-2023 IEEE International Conference on Acoustics, Speech and Signal Processing (ICASSP)*, pages 1–5. IEEE, 2023.
 69. Junichi Yamagishi, Corinna Veaux, Keiichiro Oura MacDonald, et al. Cstr vctk corpus: English multi-speaker corpus for cstr voice cloning toolkit (version 0.92). University of Edinburgh. The Centre for Speech Technology Research (CSTR), 2019.
 70. Dongchao Yang, Songxiang Liu, Rongjie Huang, Jinchuan Tian, Chao Weng, and Yuexian Zou. Hifi-codec: Group-residual vector quantization for high fidelity audio codec. *arXiv preprint arXiv:2305.02765*, 2023.
 71. Reo Yoneyama, Yi-Chiao Wu, and Tomoki Toda. Source-filter hifi-gan: Fast and pitch controllable high-fidelity neural vocoder. In *ICASSP 2023-2023 IEEE International Conference on Acoustics, Speech and Signal Processing (ICASSP)*, pages 1–5. IEEE, 2023.
 72. Neil Zeghidour, Alejandro Luebs, Ahmed Omran, Jan Skoglund, and Marco Tagliasacchi. Soundstream: An end-to-end neural audio codec. *IEEE/ACM Transactions on Audio, Speech, and Language Processing*, 30:495–507, 2021.
 73. Xin Zhang, Dong Zhang, Shimin Li, Yaqian Zhou, and Xipeng Qiu. Speechn tokenizer: Unified speech tokenizer for speech large language models. *arXiv preprint arXiv:2308.16692*, 2023.